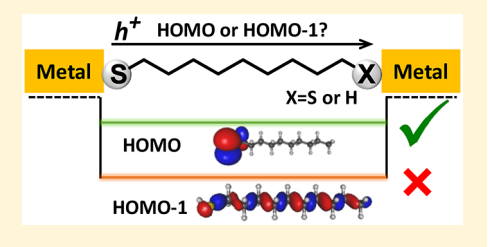


# **Energy Level Alignment in Molecular Tunnel Junctions by Transport** and Spectroscopy: Self-Consistency for the Case of Alkyl Thiols and Dithiols on Ag, Au, and Pt Electrodes

Zuoti Xie, <sup>‡</sup> Ioan Bâldea, \*, <sup>\$</sup> and C. Daniel Frisbie \*, <sup>‡</sup>

Supporting Information

ABSTRACT: We report here an extensive study of transport and electronic structure of molecular junctions based on alkyl thiols (CnT; n = 7, 8, 9, 10, 12) and dithiols (CnDT; n = 8, 9, 10) with various lengths contacted with different metal electrodes (Ag, Au, Pt). The dependence of the low-bias resistance (R) on contact work function indicates that transport is HOMO-assisted (p-type transport). Analysis of the current-voltage (I-V) characteristics for CnT and CnDT tunnel junctions with the analytical single-level model (SLM) provides both the HOMO-Fermi energy offset  $\varepsilon_{\rm h}^{\rm trans}$  and the average molecule-electrode



coupling  $(\Gamma)$  as a function of molecular length (n), electrode work function  $(\Phi)$ , and the number of chemical contacts (one or two). The SLM analysis reveals a strong Fermi level  $(E_{\rm F})$  pinning effect in all the junctions, i.e.,  $\varepsilon_{\rm h}^{\rm trans}$  changes very little with n,  $\Phi$ , and the number of chemical contacts, but  $\Gamma$  depends strongly on these variables. Significantly, independent measurements of the HOMO-Fermi level offset  $(\varepsilon_h^{UPS})$  by ultraviolet photoelectron spectroscopy (UPS) for CnT and CnDT SAMs agree remarkably well with the transport-estimated  $\varepsilon_{\rm h}^{\rm trans}$ . This result provides strong evidence for hole transport mediated by localized HOMO states at the Au-thiol interface, and not by the delocalized  $\sigma$  states in the C-C backbones, clarifying a long-standing issue in molecular electronics. Our results also substantiate the application of the single-level model for quantitative, unified understanding of transport in benchmark molecular junctions.

# ■ INTRODUCTION

One of the central focuses of molecular electronics is relating transport properties to the electronic structures of molecular junctions. 1-16 Junctions based on alkyl thiols (CnT) and dithiols (CnDT) are among the most investigated systems in molecular electronics. 17-30 However, many aspects of tunneling in these systems have been controversial and are unresolved. One fundamental question concerns which orbital (or orbitals) dominates the charge transport through CnT and CnDT. Most researchers in the molecular electronics community agree that tunneling transport for metal-alkyl (di)thiol-metal junctions is mediated by occupied states, 31-36 yet a few papers identify unoccupied states instead. 37,38 Additionally, there are substantial discrepancies between the tunneling barriers extracted from transport data, often obtained by fitting to the Simmons model, and the independently measured highest occupied molecular orbital (HOMO) positions for CnT self-assembled monolayers (SAMs) obtained by ultraviolet photoelectron spectroscopy (UPS).38-40 Some workers have ascribed this disagreement to the role of multiple orbitals participating in charge transport. 2,34,41 Tunneling barriers reported by fitting the transport data to the Simmons<sup>31,32,42-49</sup> or other barrier models<sup>50-52</sup> unfortunately also exhibit relatively large variations, typically  $\sim 1-5$  eV.

To determine which orbital is responsible for the charge transport in CnT- and CnDT-based molecular junctions, it is ideal to have a more accurate model to predict a reliable value of the tunneling barrier that can be compared directly to the UPS-measured value. Fitting transport data to the Simmons square barrier model usually requires adjusting several parameters to obtain agreement between the theoretical and experimental I-V curves. As a result, different tunneling barriers can be obtained from the same I-V curve, which results in a large variation of reported values, as just noted. Perhaps more importantly, such barrier models neglect the molecular characteristics of molecular junctions, in particular the junction electronic structure shown schematically in Figure 1A. Additionally, it has been demonstrated that analytical theories such as the Simmons model are actually incompatible with the experimental data obtained in our laboratory by the conducting probe atomic force microscopy (CP-AFM) technique<sup>31</sup> and cannot accurately fit the I-V curves of molecular junctions. <sup>34,42,53-55</sup> Recent work by the authors <sup>36,56-62</sup> has shown that the compact, analytical singlelevel model (SLM), derived from the Landauer picture and assuming that the broadening of the principal transport orbital

Received: August 18, 2019 Published: October 16, 2019



<sup>&</sup>lt;sup>‡</sup>Department of Chemical Engineering and Materials Science, University of Minnesota, Minneapolis, Minnesota 55455, United

<sup>§</sup>Theoretische Chemie, Universität Heidelberg, INF 229, D-69120 Heidelberg, Germany

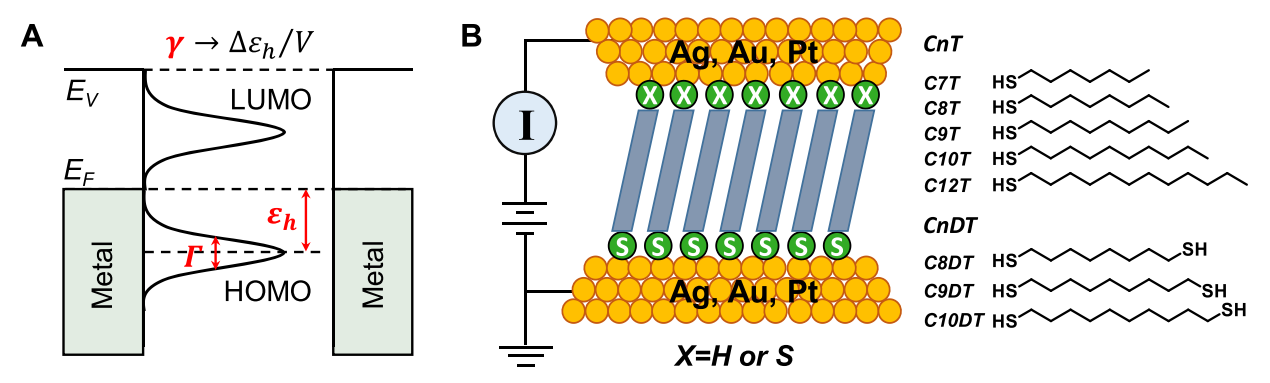


**Figure 1.** (A) Electronic structure of a molecular junction. (B) Scheme of the CP-AFM molecular junction. A metal-coated (Ag, Au, Pt) AFM tip is brought into contact with a SAM of alkyl monothiols and dithiols (CnT and CnDT) of various lengths on a metal coated substrate.

is Lorentzian, can be employed efficiently to extract the HOMO (or LUMO) position  $\varepsilon_{\rm h}^{\rm trans}$  (or  $\varepsilon_{\rm l}^{\rm trans}$ ) and the molecule–electrode coupling  $\Gamma$  from junction  $I\!-\!V$  characteristics, Figure 1A. The extraction of  $\varepsilon_{\rm h}^{\rm trans}$  and  $\Gamma$  is straightforward, without adjustable parameters.

In this Article, we employ the SLM to extract  $\varepsilon_{\rm h}^{\rm trans}$  and  $\Gamma$  for junctions based on SAMs of two series of molecules, alkyl monothiols (CnT, n = 7, 8, 9, 10, 12) and alkyl dithiols (CnDT, n = 8, 9, 10), on Ag, Au, and Pt electrodes, Figure 1B. We then compare  $\varepsilon_h^{\text{trans}}$  obtained from the transport analysis with  $\varepsilon_h^{\text{UPS}}$  measured independently by UPS for SAMs of CnDT and CnT on Ag, Au, and Pt. From UPS spectra, we find the energy states are  $\sim 1-1.5$  eV below the Fermi level (we refer to these states as the HOMO) of CnT and CnDT SAMs. The UPS values  $arepsilon_{
m h}^{
m UPS}$  are remarkably close to the transport-derived  $\varepsilon_{\rm h}^{\rm trans}$ . The agreement of the two measurements of  $\varepsilon_{\rm h}$  for 24 different types of junctions has two important consequences: (1) it provides important insight into the energy level alignment problem for CnDT and CnT with one contact vs two; (2) it confirms the SLM as a valuable theoretical tool for self-consistent analysis of I-V characteristics of alkyl thiol and dithiol based molecular junctions.

While as noted above junctions based on alkyl thiol and dithiol systems have been extensively studied in molecular electronics, UPS analysis and a comparison of  $\varepsilon_{\rm h}^{\rm trans}$  versus  $\varepsilon_{\rm h}^{\rm UPS}$  for CnT and CnDT have not been reported previously. This constitutes a new and important aspect of the current study that significantly advances the quantitative and unified understanding of these benchmark molecular junctions. We note that we have shown recently that the SLM applies well to molecular junctions based on aromatic oligophenylene thiol and dithiol (OPT and OPD) SAMs with delocalized frontier orbitals. The current work expands and complements that recent study by establishing that SLM also provides quantitative understanding of aliphatic junctions with very localized frontier orbitals.

## **■ EXPERIMENTAL SECTION**

**Materials.** In this study, we investigated alkyl monothiols (CnT), n=7, 8, 9, 10, 12 and alkyl dithiols (CnDT), n=8, 9, 10. 1-Heptanethiol (C7T, 98%), 1-octanethiol (C8T, 98.5%), 1-nonanethiol (C9T, 99%), 1-decanethiol (C10T, 99%), 1-dodecanethiol (C12T, 98%), 1,8-octanedithiol (C8DT, 97%), and 1,9-nonanedithiol (C9DT, 95%) were obtained commercially from Sigma-Aldrich, and 1,10-decanedithiol (C10DT, 99%) was obtained from TCI America. Au nuggets (99.999% pure) and Ag pellets (99.99% pure) were purchased from Mowrey, Inc. (St. Paul, MN) and Kurt J. Lesker Co., respectively. Cr evaporation rods were secured from R. D. Mathis

(Long Beach, CA). Pt and Ti metal for e-beam evaporation were purchased from Kamis, Inc. (Mahopac Falls, NY). Si (100) wafers were acquired from WaferNet (San Jose, CA). AFM tips (DNP-10  $\mathrm{Si}_3\mathrm{N}_4$  contact-mode probes) were purchased from Bruker.

Conducting Tip and Substrate Preparation. Contact-mode AFM tips were coated with Au or Ag using a thermal evaporator housed in a  $N_2$ -filled glovebox ( $H_2O$ ,  $O_2 < 0.1$  ppm). 500 Å films were deposited at a rate of 0.5-1.0 Å/s on top of a 50 Å Cr adhesion layer, and were immediately transferred without exposure to air to another glovebox containing the CP-AFM to carry out the conductance measurements. Pt films, 200 Å thick, were e-beam deposited on a 50 Å Ti adhesion layer, and immediately transferred to the measurement glovebox. The radius of the tip was ~50 nm after metal coating. Template-stripped flat metal substrates were employed to grow high-quality SAMs. For flat Ag or Au substrates, 5000 Å of Ag or Au was first deposited onto clean Si wafers in an e-beam evaporator. Si chips (1 cm<sup>2</sup>) were then glued onto the metal surface using epoxy (EPOTEK 377, Epoxy Technologies, MA). The epoxy layer was cured by placing the wafers in an oven at 120 °C for 1 h. For flat Pt substrates, 3000 Å of Pt was sputter-coated onto a clean Si wafer at a rate of ~3 Å/s. On top of the Pt film, subsequent deposition of 300 Å of Cr and 2000 Å of Au was carried out in a thermal evaporator. Note that the Cr layer prevented the penetration of Au atoms into the Pt film. The Au film enhanced the yield of flat Pt substrates due to better adhesion with the cured epoxy layer. The rest of the steps were the same as for flat Ag and Au substrates.

**Monolayer Growth and Characterization.** SAMs were formed by immersing template-stripped flat metal substrates into 1 mM ethanol solutions of the molecules for 20 h. Thicknesses of the SAMs were measured by variable angle spectroscopic ellipsometry (J. A. Woollam Co., Inc.). Briefly, the polarization angles ( $\Psi$  and  $\Delta$ ) were recorded as a function of wavelength ( $\lambda$ ) from 800 to 1100 nm with 15 nm steps and an incident angle of 65° from surface normal (Figure S1 in the Supporting Information). The HOMO-Fermi level offset of CnT and CnDT SAMs on metals was measured by UPS (Supporting Information). During UPS acquisition, -5 V was applied to the sample to obtain the secondary electron cutoff. Details of the UPS measurements are described in the Supporting Information.

**Transport Measurements.** Conductance measurements were completed by mounting the substrates in the AFM and bringing the metal-coated tip into contact with the SAM under an applied compressive load of  $\sim 1$  nN, Figure 1. The AFM instrument was installed in an Ar-filled glovebox (H<sub>2</sub>O, O<sub>2</sub> <0.1 ppm). The voltages were applied to the tip with a Keithley model 236 source-measure unit operated in "DC mode". Voltage was swept at the tip, the substrate was grounded, and I-V characteristics were recorded; V>0 means a positive voltage applied to the tip.

All measured I-V curves were linear at low biases and nonlinear at higher biases. The inverse slope of the linear portion of the I-V characteristic defined the low-bias junction resistance. The tunneling efficiency parameter  $\beta$  and contact resistance  $R_{\rm c}$  were extracted from semilog plots of the low-bias resistance versus molecule length. The

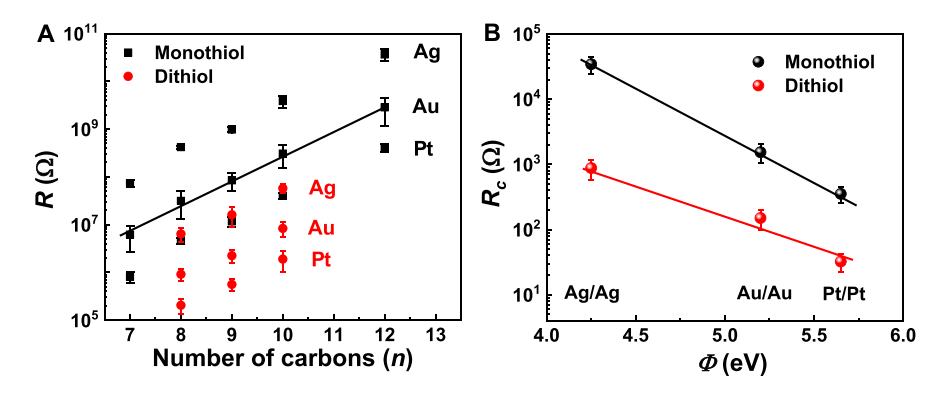


Figure 2. (A) Semilogarithmic plot of low bias resistances of CnT and CnDT junctions versus the repeat units, n. (B) Semilogarithmic plot of contact resistance of CnT and CnDT junctions versus the work functions of the bare electrodes.

Table 1. Key Electronic Structure Parameters, Including the Energy Offset  $\varepsilon_h^{\text{trans}}$ , Conductance of Junctions G, Average Coupling  $\Gamma$ , and Orbital Voltage Shift Coefficient  $\gamma$  for CnT and CnDT via the Single-Level Model (Transport)<sup>a</sup>

metal	quantity	C7T	C8T	С9Т	C10T	C12T	C8DT	C9DT	C10DT
Ag	G	$1.45 \times 10^{-8}$	$2.38 \times 10^{-9}$	$1.02 \times 10^{-9}$	$2.59 \times 10^{-10}$	$2.74 \times 10^{-11}$	$1.56 \times 10^{-7}$	$6.21 \times 10^{-8}$	$1.74 \times 10^{-8}$
	$arepsilon_{ m h}^{ m trans}$	1.19	1.13	1.14	1.13	1.14	1.23	1.22	1.26
	$arepsilon_{ m h}^{ m UPS}$	1.27	1.29	1.27	1.30	1.30	1.21	1.20	1.20
	Γ	1.92	0.75	0.49	0.25	0.08	6.20	3.85	2.12
	γ	-0.032	-0.026	-0.033	-0.039	-0.038	-0.002	0.002	-0.003
	$\Phi_{ ext{SAM}}^{ ext{UPS}}$	3.82	3.75	3.73	3.71	3.64	4.19	4.10	4.06
Au	G	$1.62 \times 10^{-7}$	$3.18 \times 10^{-8}$	$1.18 \times 10^{-8}$	$3.26 \times 10^{-9}$	$3.51 \times 10^{-10}$	$1.09 \times 10^{-6}$	$4.46 \times 10^{-7}$	$1.20 \times 10^{-7}$
	$oldsymbol{arepsilon}_{ m h}^{ m trans}$	1.01	1.01	0.94	0.97	0.97	1.12	1.07	1.08
	$arepsilon_{ m h}^{ m UPS}$	0.94	0.92	0.91	0.90	0.92	0.98	0.93	0.94
	Γ	5.50	2.45	1.41	0.75	0.25	14.88	9.07	4.74
	γ	-0.041	-0.048	-0.043	-0.044	-0.053	-0.005	-0.012	-0.005
	$\Phi_{ ext{SAM}}^{ ext{UPS}}$	4.67	4.63	4.35	4.23	4.17	4.41	4.35	4.33
Pt	G	$1.23 \times 10^{-6}$	$2.18 \times 10^{-7}$	$8.55 \times 10^{-8}$	$2.49 \times 10^{-8}$	$2.44 \times 10^{-9}$	$4.88 \times 10^{-6}$	$1.78 \times 10^{-6}$	$5.26 \times 10^{-7}$
	$arepsilon_{ m h}^{ m trans}$	0.91	0.91	0.88	0.83	0.87	0.97	0.99	0.93
	$arepsilon_{ m h}^{ m UPS}$	0.87	0.85	0.89	0.83	0.87	0.87	0.89	0.88
	Γ	13.68	5.74	3.50	1.79	0.58	27.08	16.72	8.54
	γ	-0.049	-0.053	-0.051	-0.051	-0.058	-0.002	0.004	-0.004
	$\Phi_{ ext{SAM}}^{ ext{UPS}}$	4.41	4.42	4.32	4.31	4.37	4.31	4.32	4.27

<sup>a</sup>Also included are  $\varepsilon_h^{\text{UPS}}$  and the work function for CnT and CnDT by UPS ( $\Phi_{\text{SAM}}^{\text{UPS}}$ ). Units:  $\varepsilon_h$  in eV, G in S, Γ in meV obtained from eq 3 by assuming N=70 molecules for CnT and N=80 molecules for CnDT according to the Maugis–Dugdale (MD) model of contact mechanics, <sup>60,68</sup> and Φ in eV. The UPS data have an error of ±0.1 V.

low-bias resistance was measured between  $\pm 0.1$  V except for the data of C12T, which were collected between  $\pm 0.5$  V due to its low conductivity, and sweeps up to  $\pm 1.5-2$  V were applied to the tip to obtain the transition voltage  $V_{tr}$ .

# ■ RESULTS AND DISCUSSION

Single-Level Model Analysis of CnT and CnDT Junction Transport Characteristics. Figure 2A shows the measured low-bias R data (listed in Table S1) for CnT and CnDT junctions, revealing three important aspects. First, R increases exponentially with the molecular size n, in accord with  $R_n = R_c \exp(\beta n L_0)$ , wherein the dependencies on length (n) and contact resistance ( $R_c$ ) are disentangled. This exponential dependence of CnT and CnDT junctions is well known and represents a clear indication of transport via off-resonant tunneling. S1,42 Second, R (and  $R_c$ ) dramatically decreases as the electrode work function Φ increases (Figures 2 and S2). This correlation clearly represents HOMO-mediated transport. Third, the tunneling attenuation factor β is similar for CnT and CnDT ( $\sim$ 0.9 Å $^{-1}$ ), while their  $R_c$  values

are significantly different (Figure 2B). For the electrodes studied (Ag, Au, and Pt),  $\Phi$  varies by 1.4 eV, while contact resistance decreases by a factor of 110 for monothiols and 30 for dithiols. The summary of CP-AFM measurements for CnDT SAMs associated with Figure 2 is presented in Table S1; representative results for CnT SAMs are in ref 36. The trends in Figure 2 are generally appreciated in the molecular electronics community<sup>31</sup> and are provided here as context for the new data and analysis that follow.

For a given type of electrode and the same repeat length (n), the resistance of a dithiol junction (CnDT) is smaller than the corresponding monothiol (CnT) by 1-2 orders of magnitude (Figure 2). This is true even though the CnDT is longer than the CnT with the same n due to the extra S-metal bond. The higher resistance of CnT versus CnDT junctions is ascribed to differences in the top contact (physisorbed versus chemisorbed).  $^{1,46,52,63-67}$  We note that a recent single-level model and UPS study of the energy level alignment for oligophenylene thiol- and dithiol-based (OPT and OPD)

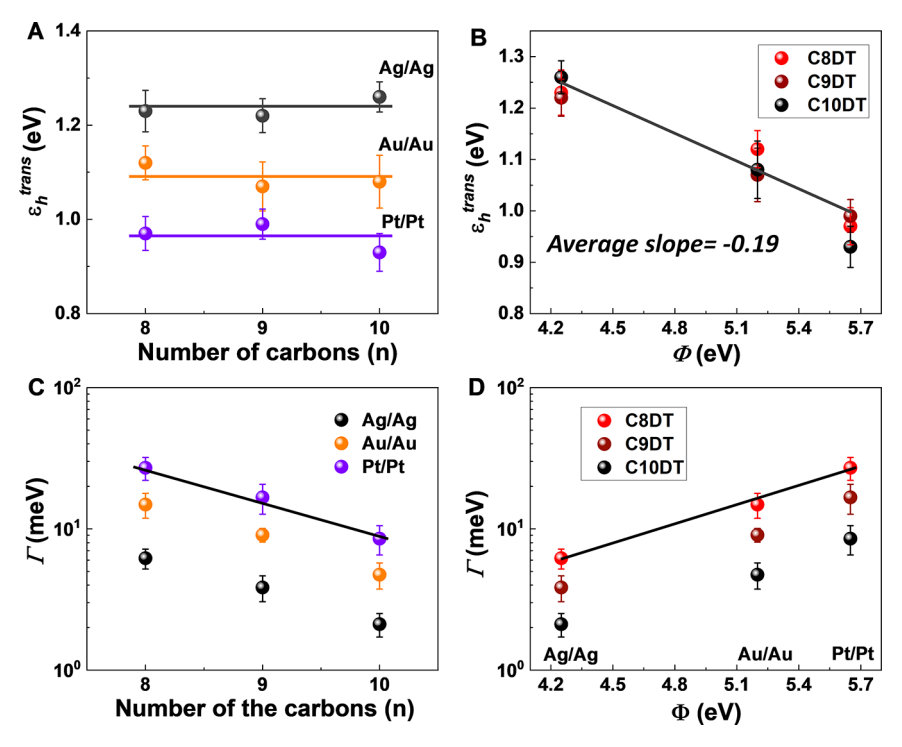


Figure 3. Energy offset  $\varepsilon_h^{trans}$  and coupling  $\Gamma$  of M-CnDT-M junctions (M = Ag, Au, Pt) as a function of (A, C) molecular length and (B, D) bare electrode work functions. The lines represent linear fits. These data are extracted from I-V traces using the SLM (see Figures S3 and S4).

junctions revealed no obvious difference in tunneling barrier; in that case, the difference in resistances was largely due to differences in  $\Gamma$ .<sup>62</sup> To address the difference in resistance between alkyl monothiol and dithiol junctions, the single-level model was applied here to analyze the general I-V behavior in the nonlinear bias range (see Figure S3). We use the transition voltage  $V_t$  values (listed in Table S1) extracted from our I-Vcurves to estimate the HOMO-Fermi energy offsets  $\varepsilon_h^{\text{trans}}$  (cf. Supporting Information). S6,57 For symmetric CnDT junctions  $(-V_{t-} = |V_{t-}| \approx V_{t+} \equiv V_t)$ , the correlation between  $V_t$  and  $\varepsilon_h$  is expressed as S6,57

$$eV_t = 2\varepsilon_{\rm h}/\sqrt{3} \tag{1}$$

and the I-V characteristics are given as

$$I = GV \frac{\varepsilon_{\rm h}^2}{\varepsilon_{\rm h}^2 - (eV/2)^2}$$
 (2)

The zero-bias conductance G = 1/R of the CP-AFM junction can be expressed as follows:

$$G = NG_0 \frac{\Gamma^2}{\varepsilon_h^2} \tag{3}$$

where  $\Gamma = \sqrt{\Gamma_s \Gamma_t} = \varepsilon_h \sqrt{G/NG_0}$  is the average interface coupling,  $\Gamma_s$  and  $\Gamma_t$  are determined by the molecular coupling to the substrate (s) and the tip (t)  $(\Gamma_s \approx \Gamma_t \text{ in symmetric})$ junctions),  $G_0 = 2e^2/h$  is the quantum conductance, and N is the number of molecules in the junction. To compute  $\Gamma$  of alkyl dithiol junctions, we set N = 80, a value close to that directly determined from other dithiol-based CP-AFM junctions.68

For asymmetric CnT junctions  $(-V_{t-} = | V_{t-} | \neq V_{t+})$ , the counterparts of eqs 1 and 2 (also deduced in ref 56) read

$$\varepsilon_{\rm h} = 2 \frac{e|V_{\rm t+}V_{\rm t-}|}{\sqrt{V_{\rm t+}^2 + 10|V_{\rm t+}V_{\rm t-}|/3 + V_{\rm t-}^2}} \tag{4}$$

$$I = GV \frac{\varepsilon_{h}^{2}}{\left[\varepsilon_{h}(V)\right]^{2} - \left(eV/2\right)^{2}}$$

$$= GV \frac{\varepsilon_{h}^{2}}{\left(\varepsilon_{h} - \gamma eV\right)^{2} - \left(eV/2\right)^{2}}$$
(5)

The orbital shift (Stark) factor  $\gamma$  is given as follows:

$$\gamma = -\frac{1}{2} \frac{V_{t+} + V_{t-}}{\sqrt{V_{t+}^2 + 10|V_{t+}V_{t-}|/3 + V_{t-}^2}}$$
 (6)

Notice that, according to eq 6,  $-V_{t-} = |V_{t-}| \neq V_{t+}$  (asymmetry) and  $\gamma \neq 0$ ; for symmetric I-V curves,  $-V_{t-} = |V_{t-}| \approx V_{t+}$  and  $\gamma$ vanishes. For asymmetric junctions, G is expressed identically to the symmetric case (eq 3).

As shown in Table 1 and Figure 3A, the HOMO energy offsets of CnDT and CnT extracted from the I-V characteristics (see Figure S3)36 are independent of the length of the molecule (n). This agrees with our quantum chemical calculations (cf. refs 36 and 59), indicating that the HOMO energies of isolated CnT and CnDT molecules are practically independent of the molecular size n. On the other hand, the HOMO energy offset slightly decreases with increasing work function of the contact metals, Figure 3B and Table 1. Specifically, for CnDT the  $\varepsilon_h^{trans}$  values change only by 0.3 eV over a 1.4 eV change in electrode work function. This is an indication of a strong Fermi level pinning effect for these junctions. This behavior is in line with our previous findings on many different types of molecular junctions. 36,58,62,65

The average contact couplings  $\Gamma$  computed from the lowbias conductance via eq 3 for CnT and CnDT junctions are

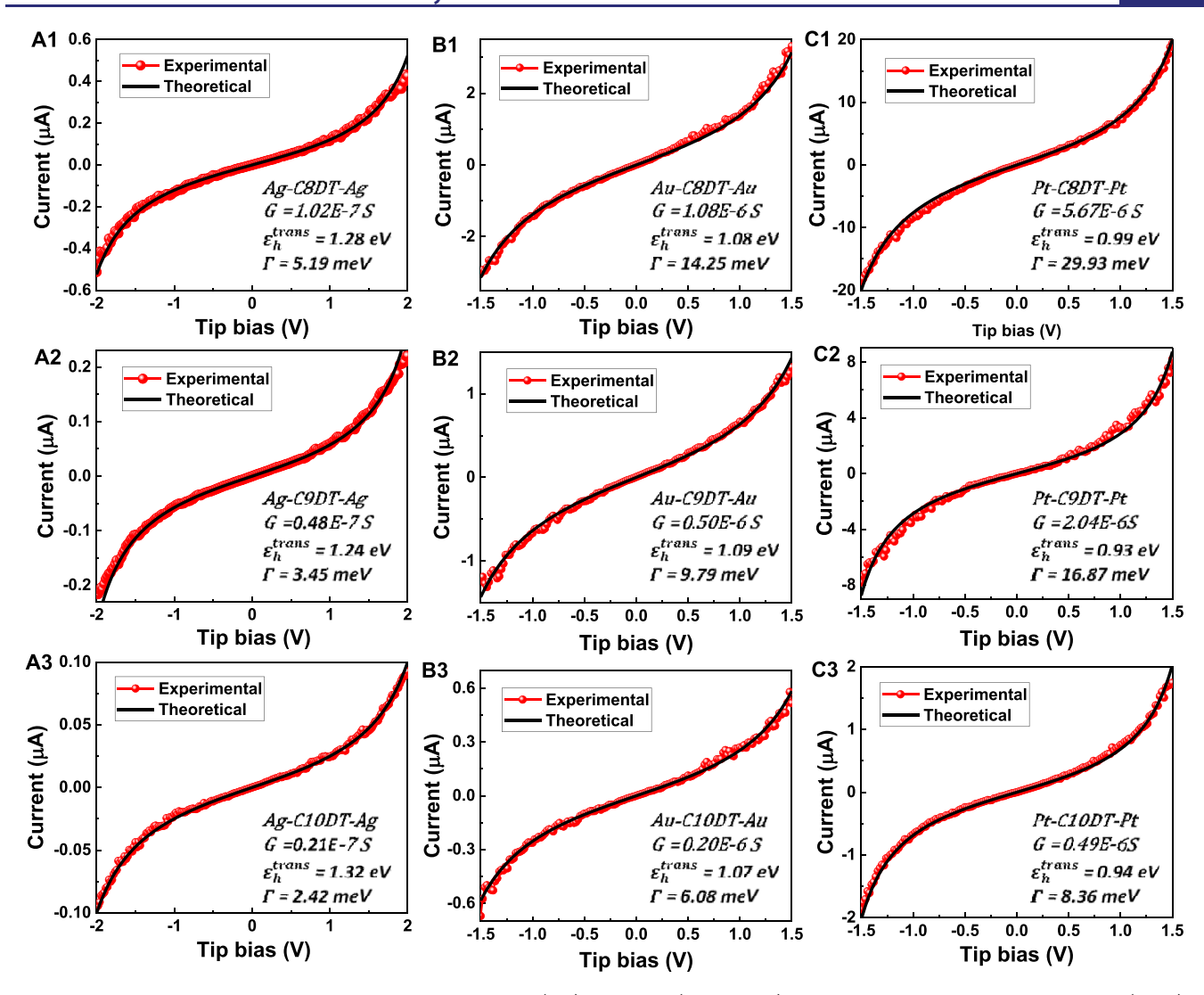


Figure 4. Comparison of the individual experimental I-V curves (red) for CnDT (n=8,9,10) and those obtained theoretically via eq 2 (black) is illustrated here for (A1–A3) Ag/Ag, (B1–B3) Au/Au, and (C1–C3) Pt/Pt junctions. The two parameters of each junction, low-bias conductance G (1/R) and the energy offset  $\varepsilon_{\rm h}$ , extracted from the I-V data, and the calculated coupling strength  $\Gamma$  for each case, are provided.

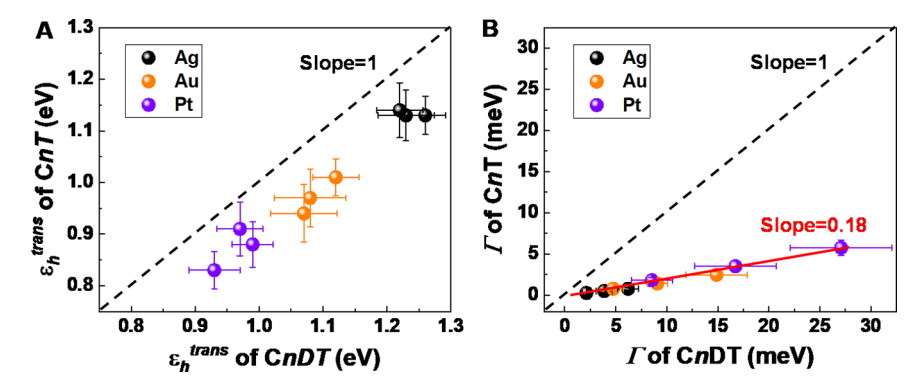


Figure 5. (A) HOMO energy offset  $\varepsilon_h^{\text{trans}}$  and (B) coupling  $\Gamma$  for CnDT vs CnT (n=8,9,10) with Ag, Au, and Pt contacts.  $\varepsilon_h^{\text{trans}}$  and  $\Gamma$  were extracted from I-V characteristics using the single-level model. The dashed lines show the slope = 1 trends for perfect correspondence. The red line in panel B represents the linear fit.

also shown in Table 1. As visualized in Figure 3C,D for CnDT junctions,  $\Gamma$  falls off exponentially (note the log scale) with n for each type of metal contact and increases exponentially with increasing  $\Phi$ . We have reported similar results earlier for CnT. The length independence of  $\varepsilon_{\rm h}^{\rm trans}$ , as well as the pinning effect resulting in small changes in  $\varepsilon_{\rm h}^{\rm trans}$  despite the

large span of contact work functions, both suggest that  $\varepsilon_{\rm h}^{\rm trans}$  cannot be responsible for the dramatic increase of R with n and the decrease of  $R_{\rm c}$  (and R) with increasing  $\Phi$ . Rather, in accord with Figure 3C,D, the strong dependence of R on n and  $\Phi$  and of  $R_{\rm c}$  on  $\Phi$  is primarily determined by the changes in  $\Gamma$ . The strong length and work function dependencies of  $\Gamma$  are

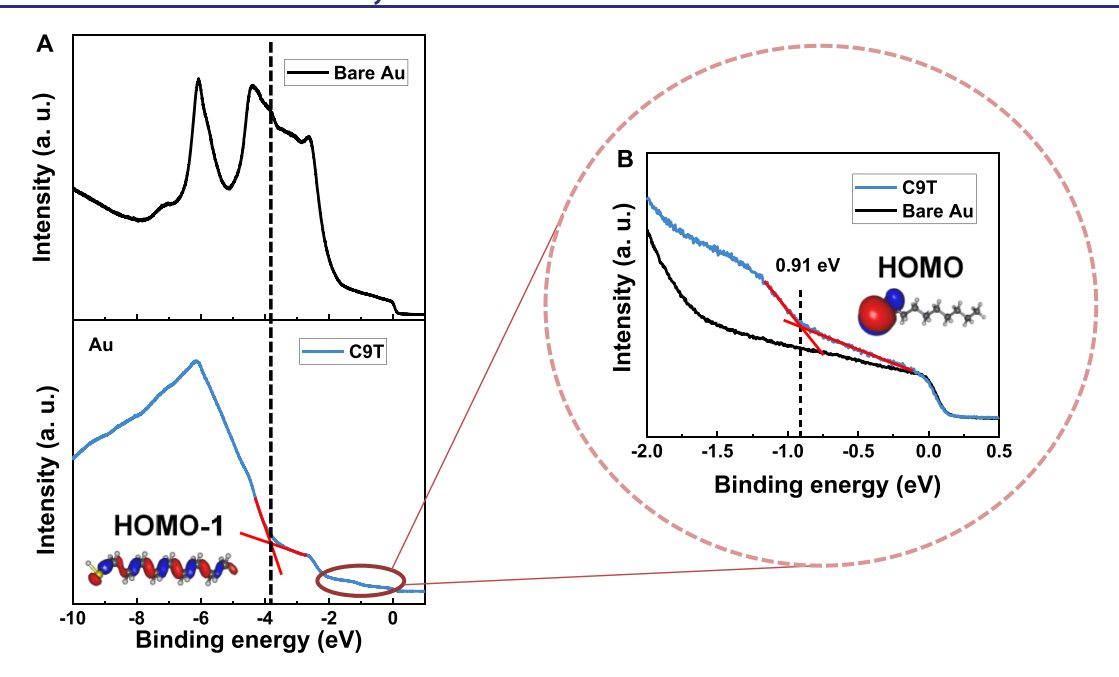


Figure 6. UPS spectra of (A) bare Au substrate and the C9T SAM modified Au substrate, and (B) the magnified spectra of bare Au and C9T/Au at low binding energy. Binding energies are referenced to the Fermi level,  $E_{\text{ref}} = E_F = 0$  eV. The spectral intensities of SAM-coated metal substrates were normalized to the intensity of bare metal substrates at 0 eV (panel B). The red intersecting lines indicate the onset energy of the HOMOs.

important characteristics of the charge transport in CnDT and CnT molecular junctions.

It can be observed in Table 1 that  $\Gamma$  for CnDT is consistently 5–8 times greater than  $\Gamma$  for CnT, depending on the metal. Because junction conductance depends on  $\Gamma^2$ , it is clear that the presence of a second metal—thiol chemical contact can increase tunneling currents by factors of  $\sim 25-64$ , which is born out in the values of G in Table 1. We return to a comparison of CnT and CnDT below.

Simulation of Full I-V Curves Using the Single-Level Model. With the model parameters  $\varepsilon_{\rm h}^{\rm trans}$  and  $\Gamma$  determined from the experimental  $V_{\rm t\pm}$  and G values via eqs 1 and 3, the I-V curves can be fully reproduced via eq 2; examples are presented in Figure 4 for  $Cn{\rm DT}$ . Similar simulations for asymmetric CnT junctions can be found in ref 36. Consistent with our previous studies,  $^{36,57-59,62}_{-59,62}$  to determine the model parameters, the full I-V curves are not "fitted"; we extract  $\varepsilon_{\rm h}^{\rm trans}$  and  $\Gamma$  as described above, and then input these values into eq 2. The excellent agreement between the simulated and experimental I-V curves represents an important self-consistency check for the model for the case of  $Cn{\rm DT}$  junctions with symmetric I-V characteristics.

Comparison of CnT and CnDT Transport. To address the difference between the resistances of CnT and CnDT junctions shown in Figure 2, we compare  $\varepsilon_h^{trans}$  and  $\Gamma$  of these two types of junctions. As shown in Figure 5A, although CnDT junctions are more conductive, the tunneling barrier of CnDT is slightly higher than that of CnT's by  $\sim$ 0.1 eV. This small increase in  $\varepsilon_h^{trans}$  obviously cannot explain the much larger conductance of CnDT compared to CnT. Thus, the difference between the cases of dithiols and monothiols traces back to  $\Gamma$ , Figure 5B, and has a clear physical interpretation.  $\Gamma$  is proportional to the square root of  $\Gamma_t$  (cf. eq 3), and  $\Gamma_t$  for monothiols is considerably smaller than for dithiols because the transfer integral between tip and the physisorbed methyl group (CnT) is substantially smaller than the transfer integral between the thiol covalently bound to the tip (CnDT).

In addition, the HOMO for alkyl thiols is quite localized near the C–S bond. <sup>36,59</sup> The fact that the HOMO distribution of the CnT molecules is concentrated at one molecular end while that of the CnDT molecules has practically equal distributions at both molecular ends, Figure S5, makes the conductance of monothiols substantially smaller than for dithiols. As discussed recently <sup>59</sup> the single-level model holds for CnDT because, although two levels (namely, HOMO and HOMO–1) contribute to the charge transport, they are nearly degenerate making their contributions practically equal.

UPS Analysis and Comparison between  $\hat{oldsymbol{arepsilon}}_{
m h}^{
m trans}$  and  $oldsymbol{arepsilon_h^{\text{UPS}}}$  . To obtain an independent measurement of  $arepsilon_h$  and to understand the role of the top contact on energy level alignment, we analyzed CnT and CnDT SAMs by UPS, which is the standard experimental method to measure the binding energies of occupied electronic states. 39,69,70 UPS measurements on alkyl monothiol SAMs on Ag and Au have been reported previously, 38-40 and the feature at ~4 eV below the Fermi level shown in Figure 6A has been assigned as the "HOMO", and is due to the C-C backbone (C-C  $\sigma$ bonding). An additional spectral feature is also seen in the UPS data for CnT on Au at a binding energy of ~1 eV below the Fermi level which has been referred to as the S-metal "interface state" at the contact, 38,39,71 Figure 6B. Our UPS measurements shown in Figure 6 and Figures S7-S10 for all samples on Ag, Au, and Pt substrates are fully consistent with these prior measurements, but it is the role of these two states near 1 and 4 eV in junction transport that must be clarified before either a comparison of  $\varepsilon_{\rm h}^{\rm trans}$  and  $\varepsilon_{\rm h}^{\rm UPS}$  can be made, or the role of the second contact on energy alignment can be

Previous molecular electronics studies on alkyl thiol junctions have suggested that transport occurs simultaneously through both channels, namely tunneling is mediated by both the "interface state", i.e., the resonance at  $\sim\!1$  eV, and the "HOMO", i.e., the  $\sim\!4$  eV deep orbital associated with the C–C  $\sigma$  backbone.  $^{34,41}$  However, in recent experimental and

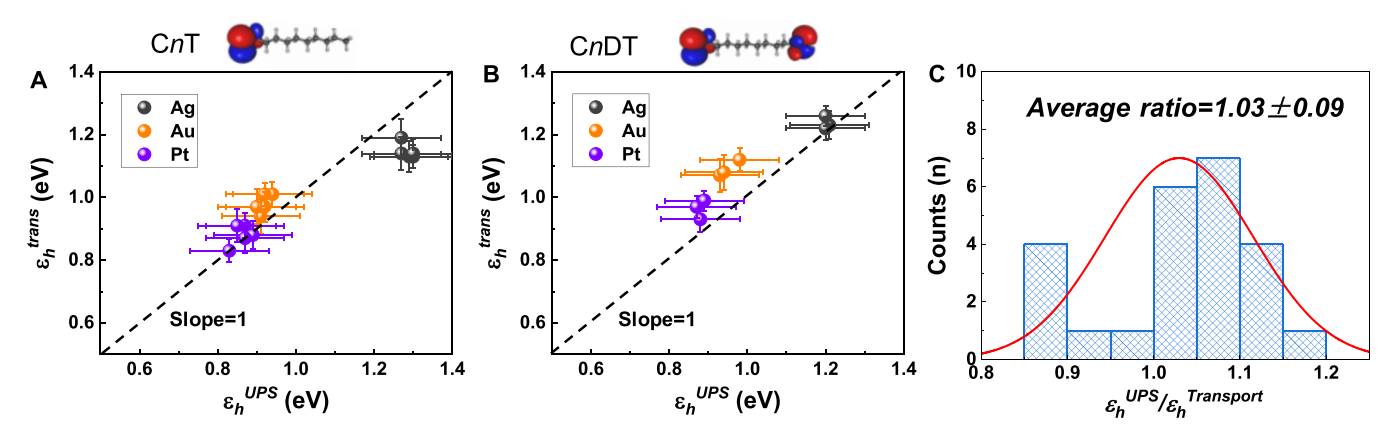


Figure 7. Comparison of  $\varepsilon_h^{trans}$  from transport measurements (and the single-level model) with  $\varepsilon_h^{UPS}$  from UPS measurements for (A) CnT and (B) CnDT molecular junctions with Ag, Au, and Pt contacts. (C) The statistical distribution of the ratio  $\varepsilon_h^{UPS}/\varepsilon_h^{trans}$  for the data in (A) and (B). The dashed lines in panels (A) and (B) show the trends for perfect correspondence.

theoretical work on CnT junctions we have eliminated the possibility that the backbone "HOMO", which we refer to here as HOMO-1 (see orbital picture in Figure 6), contributes to transport in a manner comparable to the "interface state", which we call HOMO (see Figure 6).60 Specifically, ab initio outer-valence Green's function (OVGF)<sup>72,73</sup> quantum chemical calculations as implemented in GAUSSIAN 16<sup>74</sup> using 6-311++g(d,p) basis sets<sup>75,76</sup> demonstrate that the C-C  $\sigma$ orbital, i.e., the HOMO-1 of isolated CnT and the HOMO-2 of isolated CnDT (see Figures S5 and S6), is a delocalized orbital with a length-dependent energy. In contrast, the HOMO of isolated CnT and HOMO/HOMO-1 of isolated CnDT are localized on the S end(s) of the molecules (see Figures S5 and S6) with nearly degenerate, length independent energies. In our prior work, the difference in spatial extent of these orbitals and their response to mechanical stretching in junctions allowed us to determine that the localized HOMO of CnT and HOMO/ HOMO-1 of CnDT are responsible for transport in these systems.60

The current study provides further support for this conclusion. Specifically, the length independence of the computed energies for the HOMO of isolated CnT and HOMO/HOMO-1 of isolated CnDT is in agreement with nindependent  $\varepsilon_h$  observed in our UPS and transport data for CnT and CnDT SAMs, Table 1 and Figure 3a. The substantial *n* dependence of the calculated HOMO−1 energies of isolated CnT and HOMO-2 of isolated CnDT (Figures S5 and S6) is not consistent with the experimental data. Note also that the computed n-dependence spans a range (almost 0.6 eV for CnT) substantially larger than the experimental uncertainties (~0.1 eV). Thus, the quantum chemical calculations and the current data solidify our earlier conclusion<sup>60</sup> that charge transport is not determined by the delocalized HOMO-1 (C-C  $\sigma$  orbital) for CnT junctions or by the HOMO-2 for CnDT junctions.

Parenthetically, it is also interesting to note that the delocalized HOMO-1 for isolated CnT molecules and HOMO-2 for isolated CnDT are very close to the HOMO of isolated pure alkanes (Cn; no thiols at ends), as shown in Figure S6. At large sizes ( $n \to \infty$ , equivalently  $1/n \to 0$ ) the HOMO-1 of CnT tends to the HOMO of Cn; that is, the alkane backbone is only slightly perturbed by the thiol end. Additionally, even in the limit of very large sizes  $(1/n \to 0)$ , the HOMO-1 of CnT remains substantially below the

HOMO; thus, there is little need to consider the HOMO-1 for large n in CnT molecular junctions (or the HOMO-2 for CnDT junctions).

We turn now to our central result, which is a direct comparison of  $\varepsilon_{\rm h}^{\rm trans}$  and  $\varepsilon_{\rm h}^{\rm UPS}$ . Figures S8 and S9 show magnified UPS spectra for SAMs of CnT and CnDT on Ag, Au, and Pt substrates, respectively. In these binding energy spectra, the Fermi edge is clearly visible and the HOMO onsets (near 1 eV) were established using standard protocols as indicated. The resulting 24  $\varepsilon_{\rm h}^{\rm UPS}$  values obtained by UPS for CnT and CnDT are compared to the corresponding 24  $\varepsilon_{\rm h}^{\rm trans}$  values obtained by transport, Figure 7 and Table 1. The agreement between  $\varepsilon_{\rm h}^{\rm UPS}$  and  $\varepsilon_{\rm h}^{\rm trans}$  is excellent; within error, most of the data points in Figure 7 lie on the slope = 1 trendline, i.e.,  $\varepsilon_{\rm h}^{\rm UPS}$  and  $\varepsilon_{\rm h}^{\rm trans}$  are essentially the same. Figure 7C shows the statistical distribution of the ratio  $\varepsilon_{\rm h}^{\rm UPS}/\varepsilon_{\rm h}^{\rm trans}$  for the 24 junctions.

Several important points result from comparison of  $\varepsilon_h^{UPS}$  and  $\varepsilon_{\rm h}^{\rm trans}$  for CnDT and CnT SAMs. First, the general agreement between  $arepsilon_{
m h}^{
m UPS}$  and  $arepsilon_{
m h}^{
m trans}$  is important validation of the SLM for CnT and CnDT junctions, as  $\varepsilon_h^{trans}$  is determined by SLM analysis of the experimental transport data. Self-consistency between independent measurements of  $\varepsilon_{\rm h}$ —i.e., transport and electron spectroscopy here—is gratifying and extremely rare in molecular electronics, but it is necessary if the field is to move to a more quantitative footing. Our findings here also complement our recent findings on aromatic systems, which together demonstrate that the SLM model can apply equally well to junctions with localized or delocalized transport orbitals. Second, the agreement between  $\varepsilon_{\rm h}^{\rm UPS}$  and  $\varepsilon_{\rm h}^{\rm trans}$  is further excellent support of HOMO-only assisted transport in the case of CnT and HOMO/HOMO-1 assisted transport in the case of CnDT. A clearer physical picture of transport in these benchmark systems, and its relation to electronic structure, is an important milestone. Third, we note that  $\varepsilon_{\rm h}^{\rm UPS}$  and  $\varepsilon_{\rm h}^{\rm trans}$  agree in spite of the fact that the UPS measurement probes SAMs on one contact, whereas the molecular junction has two contacts, and this has important implications for the mechanism of energy level alignment. Evidently, binding of a CnT or CnDT molecule to a metal via a single thiol group essentially fixes  $\varepsilon_{\rm h}$ ; introducing a second, chemically or physically bonded metal contact has a minimal impact on  $\varepsilon_{\rm h}$ . This is consistent with the fact that very similar  $\varepsilon_{\rm h}^{\rm trans}$  values are found for both CnDT and CnT junctions. The negligible impact of the second contact on  $\varepsilon_{\rm h}$  further implies that image charge effects must be reasonably small, as the effects of a second contact would be expected to be roughly additive.

In closing, it is interesting to speculate on the relationship of our current work to the recent results of N. J. Tao and colleagues on the electrochemical gating of an alkyl dithiol single-molecule junction.<sup>79</sup> In that work, the conductance of the C8DT alkyl dithiol was found to be independent of electrochemical gating potential. Indeed, one can suppose that the S-localized HOMO and HOMO-1 of the C8DT molecule are not susceptible to gating as these nearly degenerate states are pinned to the adjacent metal states. On the other hand, if transport were mediated by the HOMO-2 state delocalized along the C-C backbone, one might expect gating to have had an effect. It appears that the recent work of Tao is broadly consistent with our findings.

#### CONCLUSION

Utilizing molecules of various lengths n and metallic electrodes (Ag, Au, and Pt) with broadly varying work functions  $\Phi$ , we were able to assess the impact of n and  $\Phi$  on alkyl monothiol (CnT) and dithiol (CnDT) junction properties. The independence of  $\varepsilon_h$  on n and weak dependence of  $\varepsilon_h$  on the nature of the SAM-tip contact and work function implies that the n, contact, and  $\Phi$  dependence of transport is mainly determined by the electronic coupling  $\Gamma$ .

Critically, the values of  $\varepsilon_{\rm h}^{\rm UPS}$  measured by photoelectron spectroscopy are in excellent correspondence with the transport estimates  $\varepsilon_h^{\text{trans}}$  for both systems. The agreement between the SLM estimation and UPS reveals that the dominant orbital for charge transport in CnT and CnDT junctions is located at the thiol end group, i.e., localized at the end of CnT and CnDT. The agreement also substantiates the application of the single-level model to the analysis of CnT and CnDT molecular junctions. Further, the comparison of  $\varepsilon_{\rm h}^{\rm UPS}$ and  $\varepsilon_h^{\text{trans}}$  for CnT and CnDT SAMs gives important insights on the energy level alignment in these junctions, namely, that  $\varepsilon_{\rm h}$  is largely set by the metal-S bonding at the bottom contact, while the effects of the second thiol for dithiol molecules and the second top contact (and thus image charge for both thiols and dithiols) on  $\varepsilon_h$  are negligible.

Comparison of our collective results for CnT and CnDT SAMs with our previously published analysis of aromatic OPT*n* and OPD*n* SAMs<sup>62</sup> reveals anticipated differences. Specifically,  $\Gamma$  is significantly larger (up to a factor of 10) for OPTn and OPDn molecules than for CnT and CnDT of comparable molecular length. This is not surprising as the frontier orbitals (HOMOs) in the OPTn and OPDn systems are delocalized over the entire molecule whereas the HOMO in CnT and HOMO/HOMO-1 in CnDT are quite localized at the contacts. Bearing in mind that the low-bias conductance G is proportional to  $\Gamma^2$  (eq 3) the differences in  $\Gamma$  alone are nearly enough to account for the approximate factor of 100 differences in G between junctions based on aliphatic CnT and CnDT versus aromatic OPTn and OPDn. The somewhat smaller value of  $\varepsilon_h$  for the aromatic versus the aliphatic systems also contributes to the conductance difference, but the main contributor appears to be  $\Gamma$ .

Overall, our study provides a self-consistent, comprehensive picture of tunneling transport in a benchmark set of aliphatic molecular junctions and adds more evidence that combining transport, electron spectroscopy, and analytical theory is a

productive strategy for quantitative analysis in molecular electronics.

## ASSOCIATED CONTENT

# S Supporting Information

The Supporting Information is available free of charge on the ACS Publications website at DOI: 10.1021/jacs.9b08905.

Experimental and theoretical details; supplementary Tables S1 and S2 and Figures S1-S10 (PDF)

#### AUTHOR INFORMATION

### **Corresponding Authors**

\*ioan.baldea@pci.uni-heidelberg.de \*frisbie@umn.edu

#### ORCID 0

Zuoti Xie: 0000-0002-1828-0122 Ioan Bâldea: 0000-0003-4860-5757 C. Daniel Frisbie: 0000-0002-4735-2228

#### Notes

The authors declare no competing financial interest.

## ACKNOWLEDGMENTS

C.D.F. acknowledges financial support from the U.S. National Science Foundation (CHE-1708173). Parts of this work were carried out in the Characterization Facility, University of Minnesota, which receives partial support from the NSF through the MRSEC program. I.B. acknowledges financial support from the Deutsche Forschungsgemeinschaft (grant BA 1799/3-2) and computational support from the State of Baden-Württemberg through bwHPC and the German Research Foundation (DFG) through grant no. INST 40/ 467-1 FUGG.80

#### REFERENCES

- (1) Heimel, G.; Romaner, L.; Zojer, E.; Brédas, J.-L. Toward Control of the Metal-Organic Interfacial Electronic Structure in Molecular Electronics: A First-Principles Study on Self-Assembled Monolayers of  $\pi$ -Conjugated Molecules on Noble Metals. Nano Lett. 2007, 7,
- (2) Quek, S. Y.; Choi, H. J.; Louie, S. G.; Neaton, J. B. Length Dependence of Conductance in Aromatic Single-Molecule Junctions. Nano Lett. 2009, 9, 3949-3953.
- (3) Van Dyck, C.; Ratner, M. A. Molecular Junctions: Control of the Energy Gap Achieved by a Pinning Effect. J. Phys. Chem. C 2017, 121, 3013-3024.
- (4) Diez-Cabanes, V.; Gonzalez, S. R.; Osella, S.; Cornil, D.; Van Dyck, C.; Cornil, J. Energy Level Alignment at Interfaces between Au (111) and Thiolated Oligophenylenes of Increasing Chain Size: Theoretical Evidence of Pinning Effects. Adv. Thorry Simulations 2018, 1, 1700020.
- (5) Jia, C.; Migliore, A.; Xin, N.; Huang, S.; Wang, J.; Yang, Q.; Wang, S.; Chen, H.; Wang, D.; Feng, B.; et al. Covalently-Bonded Single Molecule Junctions with Stable and Reversible Photoswitched Conductivity. Science 2016, 352, 1443-1445.
- (6) Li, L.; Lo, W.; Cai, Z.; Zhang, N.; Yu, L. Proton-Triggered Switch Based on a Molecular Transistor with Edge-on Gate. Chem. Sci. 2016, 7, 3137-3141.
- (7) Sangtarash, S.; Vezzoli, A.; Sadeghi, H.; Ferri, N.; O'Brien, H. M.; Grace, I.; Bouffier, L.; Higgins, S. J.; Nichols, R. J.; Lambert, C. J. Gateway State-Mediated. Nanoscale 2018, 10, 3060-3067.
- (8) Nguyen, Q. v.; Martin, P.; Frath, D.; Della Rocca, M. L.; Lafolet, F.; Barraud, C.; Lafarge, P.; Mukundan, V.; James, D.; McCreery, R. L.; Lacroix, J.-C. Control of Rectification in Molecular Junctions:

- Contact E Ff Ects and Molecular Signature. J. Am. Chem. Soc. 2017, 139, 11913–11922.
- (9) Sayed, S. Y.; Fereiro, J. A.; Yan, H.; McCreery, R. L.; Bergren, A. J. Charge Transport in Molecular Electronic Junctions: Compression of the Molecular Tunnel Barrier in the Strong Coupling Regime. *Proc. Natl. Acad. Sci. U. S. A.* **2012**, *109*, 11498–11503.
- (10) Meng, F.; Hervault, Y.-M.; Shao, Q.; Hu, B.; Norel, L.; Rigaut, S.; Chen, X. Orthogonally Modulated Molecular Transport Junctions for Resettable Electronic Logic Gates. *Nat. Commun.* **2014**, *5*, 3023.
- (11) Kim, T.; Darancet, P.; Widawsky, J. R.; Kotiuga, M.; Quek, S. Y.; Neaton, J. B.; Venkataraman, L. Determination of Energy Level Alignment and Coupling Strength in 4,4′-Bipyridine Single-Molecule Junctions. *Nano Lett.* **2014**, *14*, 794–798.
- (12) Ting, T. C.; Hsu, L. Y.; Huang, M. J.; Horng, E. C.; Lu, H. C.; Hsu, C. H.; Jiang, C. H.; Jin, B. Y.; Peng, S. M.; Chen, C. H. Energy-Level Alignment for Single-Molecule Conductance of Extended Metal-Atom Chains. *Angew. Chem., Int. Ed.* **2015**, *54*, 15734–15738.
- (13) Yuan, L.; Nerngchamnong, N.; Cao, L.; Hamoudi, H.; del Barco, E.; Roemer, M.; Sriramula, R. K.; Thompson, D.; Nijhuis, C. A. Controlling the Direction of Rectification in a Molecular Diode. *Nat. Commun.* **2015**, *6*, 6324.
- (14) Aragones, A. C.; Aravena, D.; Cerda, J. I.; Acís-Castillo, Z.; Li, H.; Real, J. A.; Sanz, F.; Hihath, J.; Ruiz, E.; Díez-Pérez, I. Large Conductance Switching in a Single-Molecule Device through Room Temperature Spin-Dependent Transport. *Nano Lett.* **2016**, *16*, 218–226.
- (15) Guo, C.; Yu, X.; Refaely-Abramson, S.; Sepunaru, L.; Bendikov, T.; Pecht, I.; Kronik, L.; Vilan, A.; Sheves, M.; Cahen, D. Tuning Electronic Transport via Hepta-Alanine Peptides Junction by Tryptophan Doping. *Proc. Natl. Acad. Sci. U. S. A.* **2016**, *113*, 10785–10790.
- (16) Xiang, L.; Palma, J. L.; Li, Y.; Mujica, V.; Ratner, M. A.; Tao, N. J. Gate-Controlled Conductance Switching in DNA. *Nat. Commun.* **2017**, *8*, 14471.
- (17) Boulas, C.; Davidovits, J. V.; Rondelez, F.; Vuillaume, D. Suppression of Charge Carrier Tunneling through Organic Self-Assembled Monolayers. *Phys. Rev. Lett.* **1996**, *76*, 4797–4800.
- (18) Cui, X. D.; Primak, A.; Zarate, X.; Tomfohr, J.; Sankey, O. F.; Moore, A. L.; Moore, T. A.; Gust, D.; Harris, G.; Lindsay, S. M. Reproducible Measurement of Single-Molecule Conductivity. *Science* **2001**, 294, 571–574.
- (19) Wierzbinski, E.; Yin, X.; Werling, K.; Waldeck, D. H. The Effect of Oxygen Heteroatoms on the Single Molecule Conductance of Saturated Chains. *J. Phys. Chem. B* **2013**, *117*, 4431–4441.
- (20) Bâldea, I.; Xie, Z.; Frisbie, C. D. Uncovering a Law of Corresponding States for Electron Tunneling in Molecular Junctions. *Nanoscale* **2015**, *7*, 10465–10471.
- (21) Jiang, L.; Sangeeth, C. S. S.; Nijhuis, C. A. The Origin of the Odd Even Effect in the Tunneling Rates across EGaIn Junctions with Self-Assembled Monolayers (SAMs) of n Alkanethiolates. *J. Am. Chem. Soc.* **2015**, *137*, 10659–10667.
- (22) Jeong, H.; Kim, D.; Xiang, D.; Lee, T. High-Yield Functional Molecular Electronic Devices. ACS Nano 2017, 11, 6511–6548.
- (23) Salomon, A.; Cahen, D.; Lindsay, S.; Tomfohr, J.; Engelkes, V. B.; Frisbie, C. D. Comparison of Electronic Transport Measurements on Organic Molecules. *Adv. Mater.* **2003**, *15*, 1881–1890.
- (24) Chen, F.; Li, X.; Hihath, J.; Huang, Z.; Tao, N. J. Effect of Anchoring Groups on Single-Molecule Conductance: Comparative Study of Thiol-, Amine-, and Carboxylic-Acid-Terminated Molecules. *J. Am. Chem. Soc.* **2006**, *128*, 15874–15881.
- (25) Long, D. P.; Lazorcik, J. L.; Mantooth, B. A.; Moore, M. H.; Ratner, M. A.; Troisi, A.; Yao, Y.; Ciszek, J. W.; Tour, J. M.; Shashidhar, R. Effects of Hydration on Molecular Junction Transport. *Nat. Mater.* **2006**, *5*, 901–908.
- (26) Nijhuis, C. A.; Reus, W. F.; Whitesides, G. M. Molecular Rectification in Metal-SAM-Metal Oxide-Metal Junctions. *J. Am. Chem. Soc.* **2009**, *131*, 17814–17827.

- (27) Lee, W.; Reddy, P. Creation of Stable Molecular Junctions with a Custom-Designed Scanning Tunneling Microscope. *Nanotechnology* **2011**, 22, 485703.
- (28) Thuo, M. M.; Reus, W. F.; Nijhuis, C. A.; Barber, J. R.; Kim, C.; Schulz, M. D.; Whitesides, G. M. Odd Even Effects in Charge Transport across Self-Assembled Monolayers. *J. Am. Chem. Soc.* **2011**, 133, 2962–2975.
- (29) Cheng, Z.-L.; Skouta, R.; Vazquez, H.; Widawsky, J. R.; Schneebeli, S.; Chen, W.; Hybertsen, M. S.; Breslow, R.; Venkataraman, L. In Situ Formation of Highly Conducting Covalent Au-C Contacts for Single-Molecule Junctions. *Nat. Nanotechnol.* **2011**, *6*, 353–357.
- (30) Kronemeijer, A. J.; Katsouras, I.; Huisman, E. H.; van Hal, P. A.; Geuns, T. C. T.; Blom, P. W. M.; de Leeuw, D. M. Universal Scaling of the Charge Transport in Large-Area Molecular Junctions. *Small* **2011**, *7*, 1593–1598.
- (31) Engelkes, V. B.; Beebe, J. M.; Frisbie, C. D. Length-Dependent Transport in Molecular Junctions Based on SAMs of Alkanethiols and Alkanedithiols: Effect of Metal Work Function and Applied Bias on Tunneling Efficiency and Contact Resistance. *J. Am. Chem. Soc.* **2004**, *126*, 14287–14296.
- (32) Cui, X. D.; Zarate, X.; Tomfohr, J.; Sankey, O. F.; Primak, A.; Moore, A. L.; Moore, T. A.; Gust, D.; Harris, G.; Lindsay, S. M. Making Electrical Contacts to Molecular Monolayers. *Nanotechnology* **2002**, *13*, 5–14.
- (33) Song, H.; Kim, Y.; Jang, Y. H.; Jeong, H.; Reed, M. A.; Lee, T. Observation of Molecular Orbital Gating. *Nature* **2009**, *462*, 1039–1043
- (34) Malen, J. A.; Doak, P.; Baheti, K.; Tilley, T. D.; Segalman, R. A.; Majumdar, A. Identifying the Length Dependence of Orbital Alignment and Contact Coupling in Molecular Heterojunctions. *Nano Lett.* **2009**, *9*, 1164–1169.
- (35) Li, C.; Pobelov, I.; Wandlowski, T.; Bagrets, A.; Arnold, A.; Evers, F. Charge Transport in Single Au | Alkanedithiol | Au Junctions: Coordination Geometries and Conformational Degrees of Freedom. J. Am. Chem. Soc. 2008, 130, 318–326.
- (36) Xie, Z.; Bâldea, I.; Frisbie, C. D. Why One Can Expect Large Rectification in Molecular Junctions Based on Alkane Monothiols and Why Rectification Is So Modest. *Chem. Sci.* **2018**, *9*, 4456–4467.
- (37) Correa-Puerta, J.; del Campo, V.; Henriquez, R.; Esaulov, V. A.; Hamoudi, H.; Flores, M.; Haberle, P. Unoccupied Interface and Molecular States in Thiol and Dithiol Monolayers. *Langmuir* **2017**, 33, 12056–12064.
- (38) Qi, Y.; Yaffe, O.; Tirosh, E.; Vilan, A.; Cahen, D.; Kahn, A. Filled and Empty States of Alkanethiol Monolayer on Au (111): Fermi Level Asymmetry and Implications for Electron Transport. *Chem. Phys. Lett.* **2011**, *511*, 344–347.
- (39) Alloway, D. M.; Hofmann, M.; Smith, D. L.; Gruhn, N. E.; Graham, A. L.; Colorado, R.; Wysocki, V. H.; Lee, T. R.; Lee, P. A.; Armstrong, N. R. Interface Dipoles Arising from Self-Assembled Monolayers on Gold: UV Photoemission Studies of Alkanethiols and Partially Fluorinated Alkanethiols. *J. Phys. Chem. B* **2003**, *107*, 11690–11699.
- (40) Alloway, D. M.; Graham, A. L.; Yang, X.; Mudalige, A.; Colorado, R.; Wysocki, V. H.; Pemberton, J. E.; Lee, T. R.; Wysocki, R. J.; Armstrong, N. R. Tuning the Effective Work Function of Gold and Silver Using  $\omega$  -Functionalized Alkanethiols: Varying Surface Composition through Dilution and Choice of Terminal Groups. *J. Phys. Chem. C* **2009**, *113*, 20328–20334.
- (41) Salomon, A.; Boecking, T.; Seitz, O.; Markus, T.; Amy, F.; Chan, C.; Zhao, W.; Cahen, D.; Kahn, A. What Is the Barrier for Tunneling Through Alkyl Monolayers? Results from n- and p-Si–Alkyl/Hg Junctions. *Adv. Mater.* **2007**, *19*, 445–450.
- (42) Holmlin, R. E.; Haag, R.; Chabinyc, M. L.; Ismagilov, R. F.; Cohen, A. E.; Terfort, A.; Rampi, M. A.; Whitesides, G. M. Electron Transport through Thin Organic Films in Metal-Insulator-Metal Junctions Based on Self-Assembled Monolayers. *J. Am. Chem. Soc.* **2001**, *123*, 5075–5085.

- (43) Li, X.; He, J.; Hihath, J.; Xu, B.; Lindsay, S. M.; Tao, N. J. Conductance of Single Alkanedithiols: Conduction Mechanism and Effect of Molecule-Electrode Contacts. *J. Am. Chem. Soc.* **2006**, *128*, 2135–2141.
- (44) Wang, W.; Lee, T.; Reed, M. A. Mechanism of Electron Conduction in Self-Assembled Alkanethiol Monolayer Devices. *Phys. Rev. B: Condens. Matter Mater. Phys.* **2003**, *68*, No. 035416.
- (45) Wang, W.; Lee, T.; Reed, M. A. Electron Tunnelling in Self-Assembled Monolayers. *Rep. Prog. Phys.* **2005**, *68*, 523–544.
- (46) Chu, C.; Na, J.; Parsons, G. N. Conductivity in Alkylamine/Gold and Alkanethiol/Gold Molecular Junctions Measured in Molecule/Nanoparticle/Molecule Bridges and Conducting Probe Structures. J. Am. Chem. Soc. 2007, 129, 2287–2296.
- (47) Akkerman, H. B.; Naber, R. C. G.; Jongbloed, B.; van Hal, P. A.; Blom, P. W. M.; de Leeuw, D. M.; de Boer, B. Electron Tunneling through Alkanedithiol Self-Assembled Monolayers in Large-Area Molecular Junctions. *Proc. Natl. Acad. Sci. U. S. A.* **2007**, *104*, 11161–11166.
- (48) Seo, K.; Lee, H. Molecular Electron Transport Changes upon Structural Phase Transitions in Alkanethiol Molecular Junctions. *ACS Nano* **2009**, *3*, 2469–2476.
- (49) Qi, Y.; Ratera, I.; Park, J. Y.; Ashby, P. D.; Quek, S. Y.; Neaton, J. B.; Salmeron, M. Mechanical and Charge Transport Properties of Alkanethiol Self-Assembled Monolayers on a Au (111) Surface: The Role of Molecular Tilt. *Langmuir* **2008**, *24*, 2219–2223.
- (50) Hansen, K.; Brandbyge, M. Current-Voltage Relation for Thin Tunnel Barriers: Parabolic Barrier Model. *J. Appl. Phys.* **2004**, *95*, 3582–3586.
- (51) DelRio, F. W.; Steffens, K. L.; Jaye, C.; Fischer, D. A.; Cook, R. F. Elastic, Adhesive, and Charge Transport Properties of a Metal Molecule Metal Junction: The Role of Molecular Orientation, Order, and Coverage. *Langmuir* **2010**, *26*, 1688–1699.
- (52) Wang, G.; Kim, T.; Jang, Y. H.; Lee, T. Effects of Metal Molecule Contact and Molecular Structure on Molecular Electronic Conduction in Nonresonant Tunneling Regime: Alkyl versus Conjugated Molecules. J. Phys. Chem. C 2008, 112, 13010–13016.
- (53) Vilan, A. Analyzing Molecular Current-Voltage Characteristics with the Simmons Tunneling Model: Scaling and Linearization. *J. Phys. Chem. C* **2007**, *111*, 4431–4444.
- (54) Holmlin, R. E.; Ismagilov, R. F.; Haag, R.; Mujica, V.; Ratner, M. A.; Rampi, M. A.; Whitesides, G. M. Correlating Electron Transport and Molecular Structure in Organic Thin Films. *Angew. Chem.* **2001**, *113*, 2378–2382.
- (55) Simmons, J. G. Generalized Formula for the Electric Tunnel Effect between Similar Electrodes Separated by a Thin Insulating Film. J. Appl. Phys. 1963, 34, 1793–1803.
- (56) Bâldea, I. Ambipolar Transition Voltage Spectroscopy: Analytical Results and Experimental Agreement. *Phys. Rev. B: Condens. Matter Mater. Phys.* **2012**, 85, No. 035442.
- (57) Xie, Z.; Bâldea, I.; Smith, C. E.; Wu, Y.; Frisbie, C. D. Experimental and Theoretical Analysis of Nanotransport in Oligophenylene Dithiol Junctions as a Function of Molecular Length and Contact Work Function. ACS Nano 2015, 9, 8022–8036.
- (58) Smith, C. E.; Xie, Z.; Baldea, I.; Frisbie, C. D. Work Function and Temperature Dependence of Electron Tunneling through an N-Type Perylene Diimide Molecular Junction with Isocyanide Surface Linkers. *Nanoscale* **2018**, *10*, 964–975.
- (59) Xie, Z.; Bâldea, I.; Oram, S.; Smith, C. E.; Frisbie, C. D. Effect of Heteroatom Substitution on Transport in Alkane Dithiol-Based Molecular Tunnel Junctions: Evidence for Universal Behavior. *ACS Nano* 2017, 11, 569–578.
- (60) Xie, Z.; Bâldea, I.; Haugstad, G.; Frisbie, C. D. Mechanical Deformation Distinguishes Tunneling Pathways in Molecular Junctions. *J. Am. Chem. Soc.* **2019**, *141*, 497–504.
- (61) Rodriguez-Gonzalez, S.; Xie, Z.; Galangau, O.; Selvanathan, P.; Norel, L.; Van Dyck, C.; Costuas, K.; Frisbie, C. D.; Rigaut, S.; Cornil, J. HOMO Level Pinning in Molecular Junctions: Joint Theoretical and Experimental Evidence. *J. Phys. Chem. Lett.* **2018**, *9*, 2394–2403.

- (62) Xie, Z.; Bâldea, I.; Frisbie, C. D. Determination of Energy Level Alignment in Molecular Tunnel Junctions by Transport and Spectroscopy: Self-Consistency for the Case of Oligophenylene Thiols and Dithiols on Ag, Au, and Pt Electrodes. *J. Am. Chem. Soc.* **2019**, *141*, 3670–3681.
- (63) Heimel, G.; Romaner, L.; Brédas, J.-L.; Zojer, E. Interface Energetics and Level Alignment at Covalent Metal-Molecule Junctions:  $\pi$ -Conjugated Thiols on Gold. *Phys. Rev. Lett.* **2006**, *96*, 196806.
- (64) Wang, G.; Kim, T.; Lee, H.; Lee, T. Influence of Metal-Molecule Contacts on Decay Coefficients and Specific Contact Resistances in Molecular Junctions. *Phys. Rev. B: Condens. Matter Mater. Phys.* **2007**, *76*, 205320.
- (65) Kim, B.; Choi, S. H.; Zhu, X.-Y.; Frisbie, C. D. Molecular Tunnel Junctions Based on  $\pi$ -Conjugated Oligoacene Thiols and Dithiols between Ag, Au, and Pt Contacts: Effect of Surface Linking Group and Metal Work Function. *J. Am. Chem. Soc.* **2011**, *133*, 19864–19877.
- (66) Akkerman, H. B.; de Boer, B. Electrical Conduction through Single Molecules and Self-Assembled Monolayers. *J. Phys.: Condens. Matter* **2008**, 20, No. 013001.
- (67) Kim, T. W.; Wang, G.; Lee, H.; Lee, T. Statistical Analysis of Electronic Properties of Alkanethiols in Metal-Molecule-Metal Junctions. *Nanotechnology* **2007**, *18*, 315204.
- (68) Xie, Z.; Bâldea, I.; Demissie, A. T.; Smith, C. E.; Wu, Y.; Haugstad, G.; Frisbie, C. D. Exceptionally Small Statistical Variations in the Transport Properties of Metal–Molecule–Metal Junctions Composed of 80 Oligophenylene Dithiol Molecules. *J. Am. Chem. Soc.* **2017**, *139*, 5696–5699.
- (69) Braun, S.; Salaneck, W. R.; Fahlman, M. Energy-Level Alignment at Organic/Metal and Organic/Organic Interfaces. *Adv. Mater.* **2009**, *21*, 1450–1472.
- (70) Cahen, D.; Kahn, A. Electron Energetics at Surfaces and Interfaces: Concepts and Experiments. *Adv. Mater.* **2003**, *15*, 271–277
- (71) Nose, D.; Dote, K.; Sato, T.; Yamamoto, M.; Ishii, H.; Noguchi, Y. Effects of Interface Electronic Structures on Transition Voltage Spectroscopy of Alkanethiol Molecular Junctions. *J. Phys. Chem. C* **2015**, *119*, 12765–12771.
- (72) Cederbaum, L. S. One-Body Green's Function for Atoms and Molecules: Theory and Application. *J. Phys. B: At. Mol. Phys.* **1975**, 8, 290–303
- (73) von Niessen, W.; Schirmer, J.; Cederbaum, L.S. Computational Methods for the One-Particle Green's Function. *Comput. Phys. Rep.* **1984**, *1*, 57–125.
- (74) Frisch, M. J.; Trucks, G. W.; Schlegel, H. B.; Scuseria, G. E.; Robb, M. A.; Cheeseman, J. R.; Scalmani, G.; Barone, V.; Petersson, G. A.; Nakatsuji, H.; Li, X.; Caricato, M.; Marenich, A. V.; Bloino, J.; Janesko, B. G.; Gomperts, R.; Mennucci, B.; Hratchian, H. P.; Ortiz, J. V.; Izmaylov, A. F.; Sonnenberg, J. L.; Williams-Young, D.; Ding, F.; Lipparini, F.; Egidi, F.; Goings, J.; Peng, B.; Petrone, A.; Henderson, T.; Ranasinghe, D.; Zakrzewski, V. G.; Gao, J.; Rega, N.; Zheng, G.; Liang, W.; Hada, M.; Ehara, M.; Toyota, K.; Fukuda, R.; Hasegawa, J.; Ishida, M.; Nakajima, T.; Honda, Y.; Kitao, O.; Nakai, H.; Vreven, T.; Throssell, K.; Montgomery, J. A., Jr.; Peralta, J. E.; Ogliaro, F.; Bearpark, M. J.; Heyd, J. J.; Brothers, E. N.; Kudin, K. N.; Staroverov, V. N.; Keith, T. A.; Kobayashi, R.; Normand, J.; Raghavachari, K.; Rendell, A. P.; Burant, J. C.; Iyengar, S. S.; Tomasi, J.; Cossi, M.; Millam, J. M.; Klene, M.; Adamo, C.; Cammi, R.; Ochterski, J. W.; Martin, R. L.; Morokuma, K.; Farkas, O.; Foresman, J. B.; Fox, D. J. Gaussian 16, Revision B.01; Gaussian, Inc.: Wallingford, CT, 2016.
- (75) Petersson, G. A.; Bennett, A.; Tensfeldt, T. G.; Al-Laham, M. A.; Shirley, W. A.; Mantzaris, J.; et al. A Complete Basis Set Model Chemistry. I. The Total Energies of Closed-Shell Atoms and Hydrides of the First-Row Elements. *J. Chem. Phys.* **1988**, *89*, 2193–2218.
- (76) Petersson, G. A.; Al-laham, M. A. A Complete Basis Set Model Chemistry. II. Open-Shell Systems and the Total Energies of the First-Row Atoms. *J. Chem. Phys.* **1991**, *94*, 6081.

- (77) Yaffe, O.; Qi, Y.; Scheres, L.; Puniredd, S. R.; Segev, L.; Ely, T.; Haick, H.; Zuilhof, H.; Vilan, A.; Kronik, L.; et al. Charge Transport across Metal/Molecular (Alkyl) Monolayer-Si Junctions Is Dominated by the LUMO Level. *Phys. Rev. B: Condens. Matter Mater. Phys.* **2012**, *85*, No. 045433.
- (78) Souto, M.; Díez-Cabanes, V.; Yuan, L.; Kyvik, A. R.; Ratera, I.; Nijhuis, C. A.; Cornil, J.; Veciana, J. Influence of the Donor Unit on the Rectification Ratio in Tunnel Junctions Based on Donor-Acceptor SAMs Using PTM Units as Acceptors. *Phys. Chem. Chem. Phys.* **2018**, 20, 25638–25647.
- (79) Wang, H.; Wang, Z.; Wang, Y.; Hihath, J.; Chen, H.-Y.; Li, Y.; Tao, N. J. Potential Dependence of Mechanical Stability and Electronic Coupling of Single S—Au Bonds. J. Am. Chem. Soc. 2018, 140, 18074—18081.
- (80) BwHPC and BwHPC-C5, http://www.bwhpc-c5.de, funded by the Ministry of Science, Research and the Arts Baden-Württemberg, the Universities of the State Baden-Württemberg, and the German Research Foundation (DFG).